



# Preparation of Ag–Co@C–N Bimetallic Catalysts for Application to Nitroaromatic–Azoxybenzene Reduction Coupling

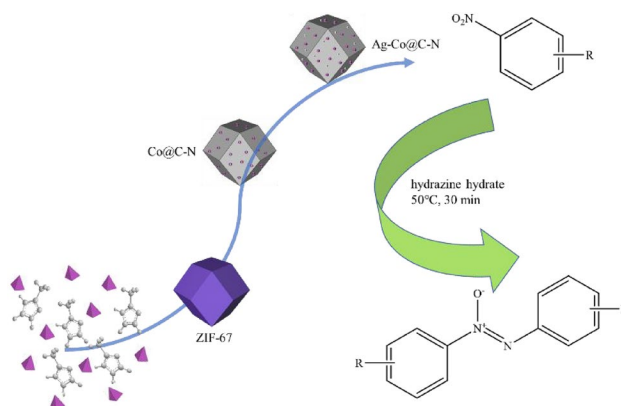
Yu Zhang<sup>1</sup> · Ying He<sup>1</sup> · Qing He<sup>1</sup> · Hui Liu<sup>1</sup> · Junfeng Miao<sup>2</sup> · Linglan Li<sup>2</sup>

Received: 5 August 2022 / Accepted: 20 February 2023 / Published online: 9 March 2023  
© The Author(s), under exclusive licence to Springer Science+Business Media, LLC, part of Springer Nature 2023

## Abstract

Selective reduction coupling of nitroaromatics to azoxybenzenes can synthesize value-added azoxybenzene downstream products. In this study, Ag–Co@C–N bimetallic catalysts with different carbonization temperatures were prepared on a metal–organic framework (MOF) template. Ag–Co bimetallic nanoparticles and carbon nanotubes were uniformly dispersed throughout Ag–Co@C–N. In the reduction of nitroaromatics to azoxybenzenes with Ag–Co@C–N, the optimized yields were 93.2% with the 100% of raw material conversion after 30 min of reaction, and no significant decrease in catalyst activity after five cycles.

## Graphical Abstract



**Keywords** Azoxybenzenes · Metal–organic frameworks · Bifunctional catalysts · Reduction

## 1 Introduction

Azoxybenzene compounds are important chemical intermediates in dyeing, organic synthesis, liquid crystals, and other applications owing to their special asymmetric structure and unique optical properties [1–5]. Azoxybenzene compounds are structurally stable in dilute acid or strong base environments, but metastable reaction intermediates are easily converted into azobenzene or other products during the reaction process. Therefore, their utility in large-scale industrial production is limited. Classical synthesis methods of azoxybenzenes include aromatic amine oxidation, reductive coupling

✉ Hui Liu  
iamliuhui@live.cn

✉ Linglan Li  
lilinglan@126.com

<sup>1</sup> Wuhan Institute of Technology Materials Science and Engineering, Wuhan 430205, China

<sup>2</sup> College of Chemistry and Chemical Engineering, Hubei University, Wuhan 430062, China

of nitroaromatics, and aromatic nitroso compounds [6–8]. The direct reductive coupling of nitroaromatics to azoxybenzenes has received special attention because nitroaromatics are structurally stable and inert to many functional groups [9, 10]. In industry, the conversion of aromatic nitro to is usually completed by adding glucose or zinc powder as a reducing agent. However, this method imposes harsh reaction conditions and seriously pollutes the environment, counteracting the drive toward green chemistry. In recent years, many efficient and mild catalytic reduction systems based on either photocatalysis or more traditional thermal catalysis have been developed. The preparation of azoxybenzenes compounds supported by metal nanoparticle catalysts has been extensively reported [11–13] because such catalysts improve the yields of traditional methods. On the downside, the product selectivity is limited by the simultaneous conversion of raw materials and over-hydrogenation of azoxybenzenes. To improve the product selectivity, many researchers have attempted structural control of catalysts.

Metal–organic frameworks (MOFs) consisting of metal nodes and organic linkers are considered as good carriers for supported carbon-based catalysts. MOFs are compositionally and structurally diverse, affording catalyst supports with ideal compositions and structures [14, 15]. Moreover, the metal elements and organic compounds in MOFs can be pyrolyzed in situ to porous carbon supports with a metal/metal oxide/metal–carbon composition, or to porous carbon without metal or nitrogen doping. The former is a suitable precursor of bifunctional catalysts, whereas the latter can act as self-sacrificing precursors/templates for the preparation of nanoporous carbon [16, 17]. MOF-derived porous carbon can inherit the structural properties and advantages of the corresponding MOF [18]. Zeolitic imidazolium frameworks (ZIFs) are particularly favorable precursor materials for the carbon base of MOF materials. ZIFs are coordination polymers composed of N-containing ligands (e.g., imidazole and its derivatives) and metal ions with a tetrahedral coordination mode (usually Zn or Co) [19, 20]. Within the zeolite-like three-dimensional topology facilitated by its intrinsic properties, the 2-methylimidazole in ZIFs generates nitrogen-doped (N-doped) carbon during pyrolysis, which enhances the mechanical strength and electron-transfer rate [21]. Therefore, ZIFs can be used as sacrificial templates in the preparation of N-doped carbon materials, and show a high development potential in other applications. In most of the existing studies on the catalytic performance of ZIFs, the structure is improved for enhancing the electron-transport efficiency of electrocatalytic reactions; the efficient catalytic reduction of nitroaromatics to azoxybenzenes using ZIFs derivatives have been rarely reported.

Herein, we prepare a novel Ag–Co@C–N bimetallic catalyst from ZIF-67 precursor and silver nanoparticles. The nanoparticles were successfully loaded by reducing silver

nitrate in ethylene glycol. The as-prepared Ag-based catalyst, Ag–Co@C–N–1000, showed high catalytic efficiency and excellent stability owing to its compositional and structural features. Nitroaromatics were completely transformed in 10 min without requiring alkaline conditions. The maximum product yield was 93.2% at 50 °C after 30 min of reaction. In addition, the cobalt nanoparticles impart a magnetic property which enables recovery by rapid separation.

## 2 Experimental Section

### 2.1 Catalyst Preparations

All reagents were of analytical grade and used without further purification.

#### 2.1.1 Preparation of ZIF-67

0.6 g  $\text{Co}(\text{NO}_3)_2 \cdot 6\text{H}_2\text{O}$  and 7.31 g 2-methylimidazole were dissolved to 4 mL and 26 mL deionized water respectively, then the first solution was slowly added to the second part, the color was rapidly turns purple, the mixture was stirred for 3 h under stirring conditions at room temperature. After the reaction was completed, the blue solid was collected by centrifugation at 8000 rpm for 4 min, followed by washing with ethanol 3 times. Then, the sample was dried under vacuum for 8 h at 60 °C to obtain ZIF-67.

#### 2.1.2 Preparation of Co@C–N

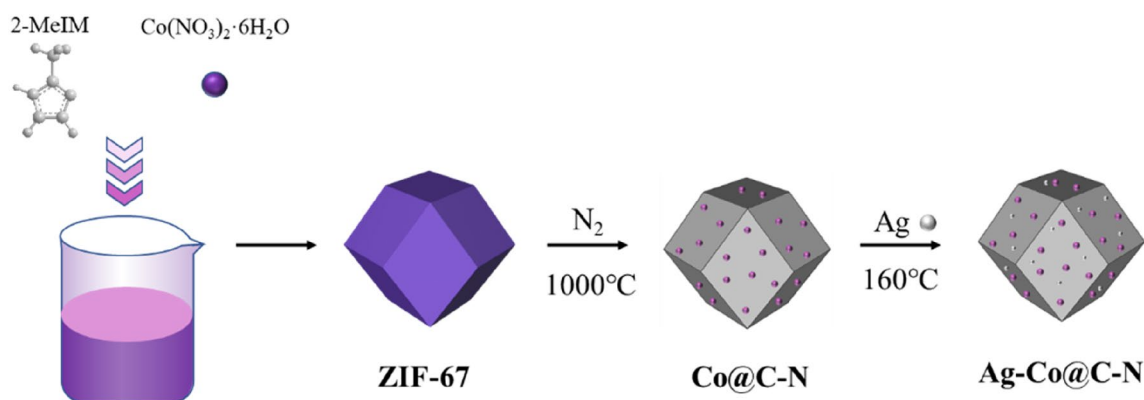
Under a  $\text{N}_2$  atmosphere, the prepared ZIF-67 was heated to different temperatures (600, 800, and 1000 °C) at 5 °C  $\text{min}^{-1}$  over 2 h, yielding a series of Co@C–N materials named Co@C–N-600, Co@C–N-800, and Co@C–N-1000.

#### 2.1.3 Preparation of Ag–Co@C–N

The Co@C–N support (0.08 g) was added to 50 mL ethylene glycol (EG). After ultrasound for 30 min, 2 mL of 0.05 mol  $\text{L}^{-1}$   $\text{AgNO}_3$ –EG solution was added and the mixed solutions were stirred at room temperature for 3 h, then refluxed at 160 °C for 3 h. The products were washed with deionized water and ethanol and dried in a vacuum at 60 °C overnight. The synthesized catalysts were named Ag–Co@C–N-600, Ag–Co@C–N-800, and Ag–Co@C–N-1000, respectively.

### 2.2 Material Characterization

The XRD patterns were recorded on a D8 Advance type X-ray powder diffractometer (Bruker, Germany) with  $\text{Cu K}_\alpha$  radiation. The operating voltage and current were 100 kV and 40 mA, respectively. The Brunauer–Emmett–Teller



**Scheme 1** Schematic showing the synthetic process of the Ag–Co@C–N

(BET) surface areas and pore structures of the samples were determined from nitrogen adsorption–desorption isotherm measurements. The morphology and elemental compositions of the as-prepared materials were observed by scanning electron microscope (SEM) (JEOL, JSW-5510LV, Japan) with energy dispersive spectroscopy (EDS) (FALCON60, USA). The morphologies of the catalysts were examined by transmission electron microscopy (TEM) (JEOL, JEM-2100, Japan). The surface states were analyzed using X-ray photoelectron spectroscopy (XPS) on an ESCALAB XI + spectrometer (Thermo Fisher Scientific, USA). The amount of Ag and Co present in Ag–Co@C–N catalysts were estimated by ICP-OES (Agilent ICPOES 730, USA). <sup>1</sup>H NMR spectroscopy was conducted in a 400/54 Premium Shielded instrument (Agilent Technologies, USA) (Scheme 1).

### 2.3 Catalytic Activity Tests

All catalytic-activity evaluation experiments were conducted in a round-bottomed flask reactor (25 mL) equipped with a condenser and magnetic stirring. Nitroaromatic (2.5 mmol) and 2wt% Ag–Co@C–N were mixed with 2.5 mL ethanol in the flask, then stirred and heated to 25–70 °C until the nitroaromatic was completely dissolved. Next, 0.5 g 80% hydrazine hydrate was added in batches to the above mixture. The reaction was run at 25–70 °C and indicated by thin-layer chromatography (TLC). Once the reaction was completed, 5 mL ethyl acetate was added and the Ag–Co/C–N was filtered off. The filtrates were concentrated in a vacuum and the residue was purified by flash column chromatography (Eluent is petroleum ether, 60–90 °C), affording the corresponding azoxybenzenes.

Each component was weighed and the nitroaromatic conversion rate (C), selectivity (S), and yield (Y) of the azoxybenzenes were respectively calculated as follows [22]:

$$C = (n_0 - n_r) / n_0 \times 100\%,$$

$$S = 2 \times n_p / (n_0 - n_r) \times 100\%,$$

$$Y = 2 \times n_p / n_0 \times 100\%,$$

where  $n_0$ ,  $n_r$ , and  $n_p$  represent the numbers of moles of initial nitroaromatic, residual nitroaromatic after the reaction, and azoxybenzenes formed, respectively.

To optimize the reaction conditions, the catalytic performances of the different catalysts were compared under different conditions (reaction temperature, reaction time, solvent, and catalyst dosage). Next, the universal applicabilities of the catalysts were tested on different substrates (1-bromo-4-nitrobenzene, nitrobenzene, 2-nitrotoluene, 3-nitrotoluene, 4-nitrotoluene, p-nitrobenzyl chloride, and 4-nitroanisole).

## 3 Results and Discussion

### 3.1 Structural Characterizations

Figure 1a shows the XRD patterns of the prepared samples. The as-prepared Co@C–N-1000 presented characteristic diffraction peaks at  $2\theta = 44.2^\circ$ ,  $51.5^\circ$ , and  $75.8^\circ$  corresponding to the (111), (200), and (220) crystal planes of  $\alpha$ -phase metallic cobalt [23], respectively. These results confirm the presence of Co in all materials. The Ag–Co@C–N-1000 composition presented characteristic peaks of Ag at  $2\theta = 38.1^\circ$ ,  $44.3^\circ$ ,  $64.4^\circ$ , and  $77.4^\circ$ , corresponding to the (111), (200), (220) and (311) crystal planes of metallic silver [24], respectively, which were absent in the XRD patterns of Co@C–N materials. It was preliminarily judged that the prepared samples were successfully loaded with the Ag and Co bicomponent metal nanoparticles and contained no valence impurities.

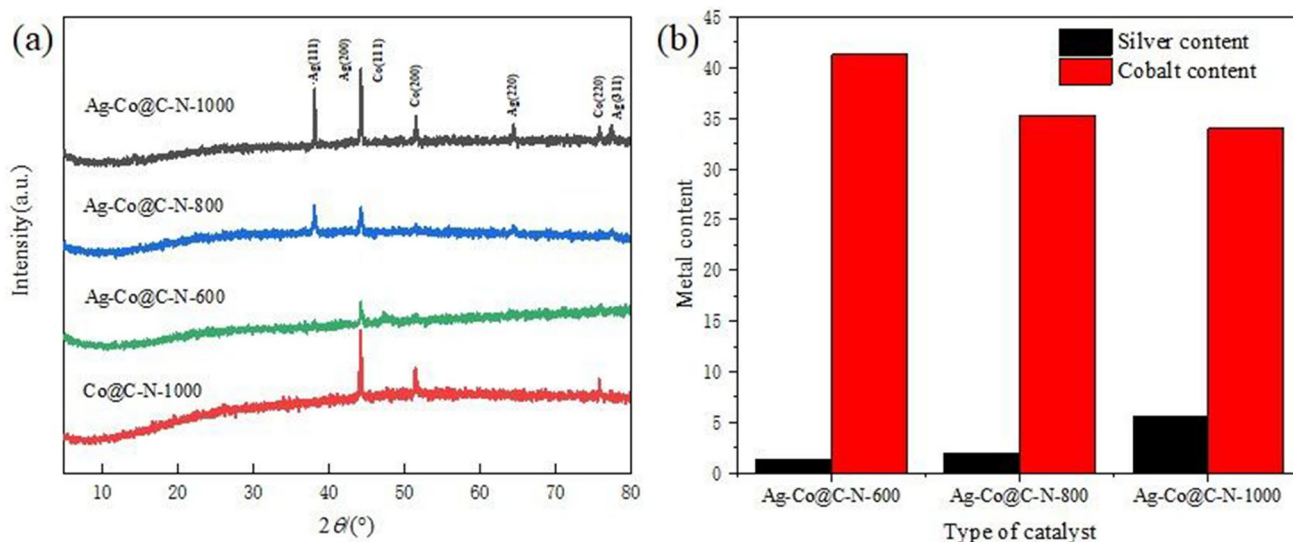


**Fig. 1** **a** XRD patterns of Co@C-N-1000, Ag-Co@C-N-600, Ag-Co@C-N-800 and Ag-Co@C-N-1000. **b** ICP-OES of Ag-Co@C-N-1000

Moreover, the results of ICP-OES (Fig. 1b) show that the content of Ag in Ag-Co@C-N-600, Ag-Co@C-N-800 and Ag-Co@C-N-1000 samples increases successively, while the cobalt content is decreasing successively. This is attributed to the fact that with the increase of carbonization temperature, the cobalt in the material will be evaporated after being reduced, resulting in more defects in the material, which cause the decrease of cobalt content and the increase of silver adsorption sites. Consequently, the Ag-Co@C-N-600 and Ag-Co@C-N-800 components displayed poorer catalytic activities than Ag-Co@C-N-1000.

The pore textural properties of the as-prepared Ag-Co@C-N-600, Ag-Co@C-N-800 and Ag-Co@C-N-1000 were determined from the N<sub>2</sub> adsorption-desorption curves shown in Fig. 2a. All three samples exhibited type IV adsorption isotherms with type H1 hysteresis loops, indicating their mesoporous structures [25, 26]. The specific surface areas (pore volumes) of Ag-Co@C-N-600, Ag-Co@C-N-800 and Ag-Co@C-N-1000 were 219 m<sup>2</sup> g<sup>-1</sup> (0.28 cm<sup>3</sup> g<sup>-1</sup>), 187 m<sup>2</sup> g<sup>-1</sup> (0.25 cm<sup>3</sup> g<sup>-1</sup>), and 163 m<sup>2</sup> g<sup>-1</sup> (0.37 cm<sup>3</sup> g<sup>-1</sup>), respectively. The N<sub>2</sub> adsorption decreases is in accordance with the specific surface area shown in Table 1. It

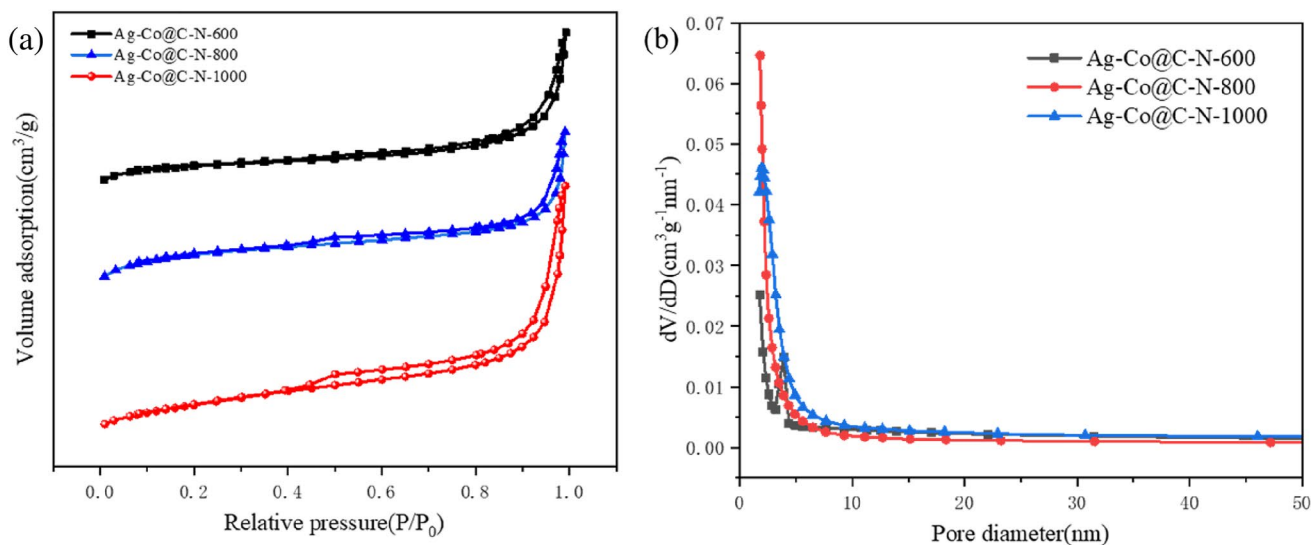


**Fig. 2** **a** Nitrogen adsorption-desorption isotherm and **b** pore size distribution of Co@C-N-1000, Ag-Co@C-N-600, Ag-Co@C-N-800 and Ag-Co@C-N-1000

**Table 1** Textural properties of Ag–Co@C–N-600, Ag–Co@C–N-800 and Ag–Co@C–N-1000

Entry	Samples	Sa BET (m <sup>2</sup> /g)	Pore volume (cm <sup>3</sup> /g)	Db p (nm)
1	Ag–Co@C–N-600	219	0.28	1.7
2	Ag–Co@C–N-800	187	0.25	1.8
3	Ag–Co@C–N-1000	163	0.37	2.1

may be attributed to the different catalytic extent of ZIF-67 [27]. The pore size distributions in Ag–Co@C–N-600, Ag–Co@C–N-800 and Ag–Co@C–N-1000 were calculated by the Barrett–Joyner–Halenda method and are plotted in Fig. 2b. The pore size distribution of Ag–Co@C–N-600 was wide whereas those of Ag–Co@C–N-800 and Ag–Co@C–N-1000 were narrower with averages of 1.78 and 2.10 nm, respectively.

Figure 3a–c displays TEM images of the Ag–Co@C–N-600, Ag–Co@C–N-800, and Ag–Co@C–N-1000 samples. Nanoparticles were observed in all samples, but were agglomerated in Ag–Co@C–N-600 and Ag–Co@C–N-800. Aggregation may have resulted from insufficient carbonization temperature, whereby ZIF-67 formed insufficiently many defects during the carbonization process to adsorb the reduced Co particles and to support the Ag nanoparticles in the subsequent preparation process; consequently, the catalytic efficiency was reduced in these two materials. Two kinds of nanoparticles were clearly observed in the Ag–Co@C–N-1000 material: one with an average length of 90–110 nm and the characteristic lattice fringes of 0.205 and 0.179 nm, which are ascribed to the (200) and (111) planes in fcc Co [28]; the other with a particle size of approximately 20 nm and the fringe spacing of 0.236 nm, corresponding to (111) planes of Ag [29]. It was preliminarily judged that the two-phase nanoparticles (Co and Ag) were successfully loaded. Clearly, the morphology of the carbon support was optimized at 1000 °C.

The morphologies and chemical compositions of the Ag–Co@C–N-1000 were observed by SEM and EDS, respectively. In the Ag–Co@C–N-1000 sample, the framework collapsed after the removal of H atoms during the carbonization process; consequently, Ag–Co@C–N-1000 exhibited uniform polyhedron morphologies with an average length and width of 140–180 and 100–150 nm, respectively (Fig. 3d). When the SEM image was combined with the TEM image in Fig. 3c, Co nanoparticles and carbon nanotubes were clearly observed on the Ag–Co@C–N-1000 surface (Fig. 3d). Because a large amount of Co<sup>2+</sup> was reduced into Co<sup>0</sup> during the high-temperature pyrolysis process, the Co<sup>0</sup> nanoparticles easily agglomerated into larger-size particles. Within the porous structure and internal defects of Co@C–N, the generated silver nanoparticles were separated

and their probability of agglomeration was reduced in the subsequent silver-nitrate reduction process. The maintenance of small Ag nanoparticles helps to improve the catalytic performance [30]. In the EDS mapping images of Ag–Co@C–N-1000 (Fig. 3e), the uniform distributions of the elements indicated the homogeneous incorporation of Ag into the Ag–Co@C–N-1000 framework.

The chemical states and elemental compositions of the as-prepared Ag–Co@C–N-1000 catalysts were characterized by XPS. The XPS spectrum of Ag–Co@C–N-1000 (Fig. 4a) displayed the peaks of C 1s, Ag 3d, and Co 2p. The detailed XPS information confirmed the presence of Ag, Co, C, and N in Ag–Co@C–N-1000, consistent with the SEM–EDS results. The Co 2p band of the catalyst (Fig. 4b) included two pairs of doublets. The first bimodal, comprising the Co 2p<sub>1/2</sub> peak at 793.9 eV and the Co 2p<sub>3/2</sub> peak at 778.6 eV, was assigned to Co<sup>0</sup> [31]. The second bimodal, composed of the Co 2p<sub>1/2</sub> peak at 796.4 eV and the Co 2p<sub>3/2</sub> peak at 780.6 eV, was assigned to Co<sup>2+</sup> [32, 33]. The two peaks in the narrow scans of Ag 3d (one at 368.7 eV, the other at 374.5 eV) were assigned to Ag<sup>0</sup> [34], confirming that Ag nanoparticles were successfully loaded without valence impurities on the Ag–Co@C–N-1000 surface (Fig. 4c). Finally, the C 1s spectrum was segmented into C–C/C=C, C–N, and C–O–C peaks located at 284.8, 285.9, and 289.5 eV, respectively.

### 3.2 Catalytic Performances

The catalytic performances of the catalysts were evaluated in the reduction of 4-chloronitrobenzene to 1,2-bis(4-chlorophenyl)diazene oxide. The results are shown in Table 2. As expected from the XRD and TEM results, the conversion rate and product yield of the raw materials were greatly improved after loading the Ag nanoparticles. The Co active component in Ag–Co@C–N-600 and Ag–Co@C–N-800 decreased because the Co nanoparticles were excessively agglomerated, reducing their final catalytic effect. Increasing the carbonization temperature to 1000 °C improved not only the conversion rate and selectivity of the raw materials but also the product yield, indicating an enhanced catalytic effect. In the reaction using the Ag–Co@C–N-1000 catalyst, the raw-material conversion rate and product yield reached 100% and 89.8% at 30 min, respectively, confirming Ag–Co@C–N-1000 as an ideal catalyst.

After determining the optimal composition of the catalyst, we optimized the catalytic reaction conditions and investigated the influences of different factors (reaction temperature, reaction time, catalyst dosage, and solvent type) on the catalytic performance. The results are shown in Table 3.

Next, the detailed effects of various reaction parameters on catalytic activity were investigated on the optimal catalyst, Ag–Co@C–N-1000. The effect of reaction temperature

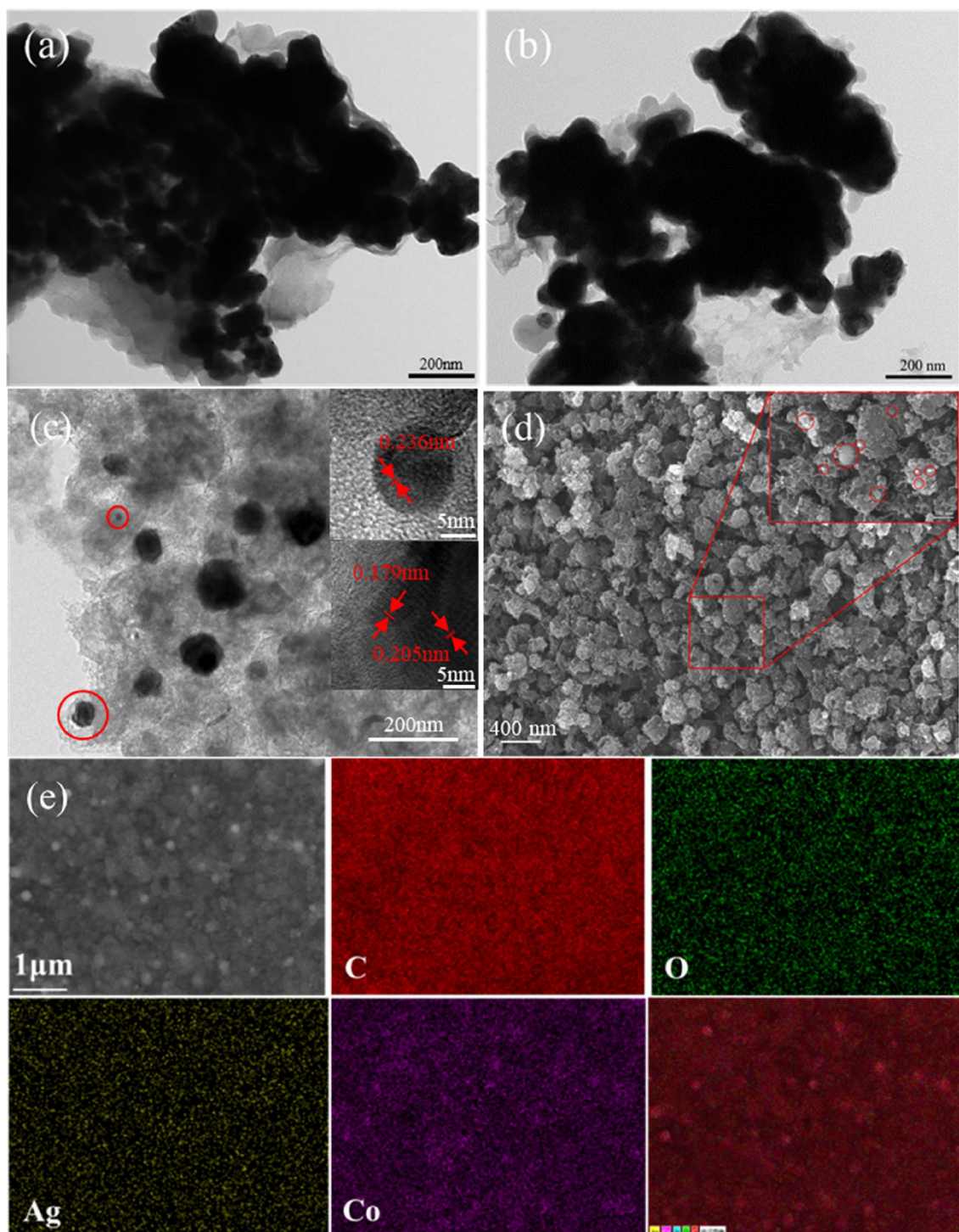


**Fig. 3** TEM images of **a** Ag-Co@C-N-600, **b** Ag-Co@C-N-800, and HRTEM images of **c** Ag-Co@C-N-1000, **d** SEM images of Ag-Co@C-N-1000, **e** EDS mapping images of Ag-Co@C-N-1000

is shown in Fig. 5. After 30 min of reaction at 25 °C, the 1,2-Bis(4-chlorophenyl)diazene oxide yield was 51.8% and the 4-nitrochlorobenzene-conversion rate was 81.0%. When the temperature was raised to 40 °C, the yield and conversion rate improved to 76.1% and 100%, respectively. Raising the

temperature to 50 °C further improved the product yield to 89.8% while the raw-material conversion rate remained at 100%. Heating decidedly improved the conversion rate of the raw materials, but the 1,2-Bis(4-chlorophenyl)diazene oxide yield began to decrease at reaction temperatures exceeding

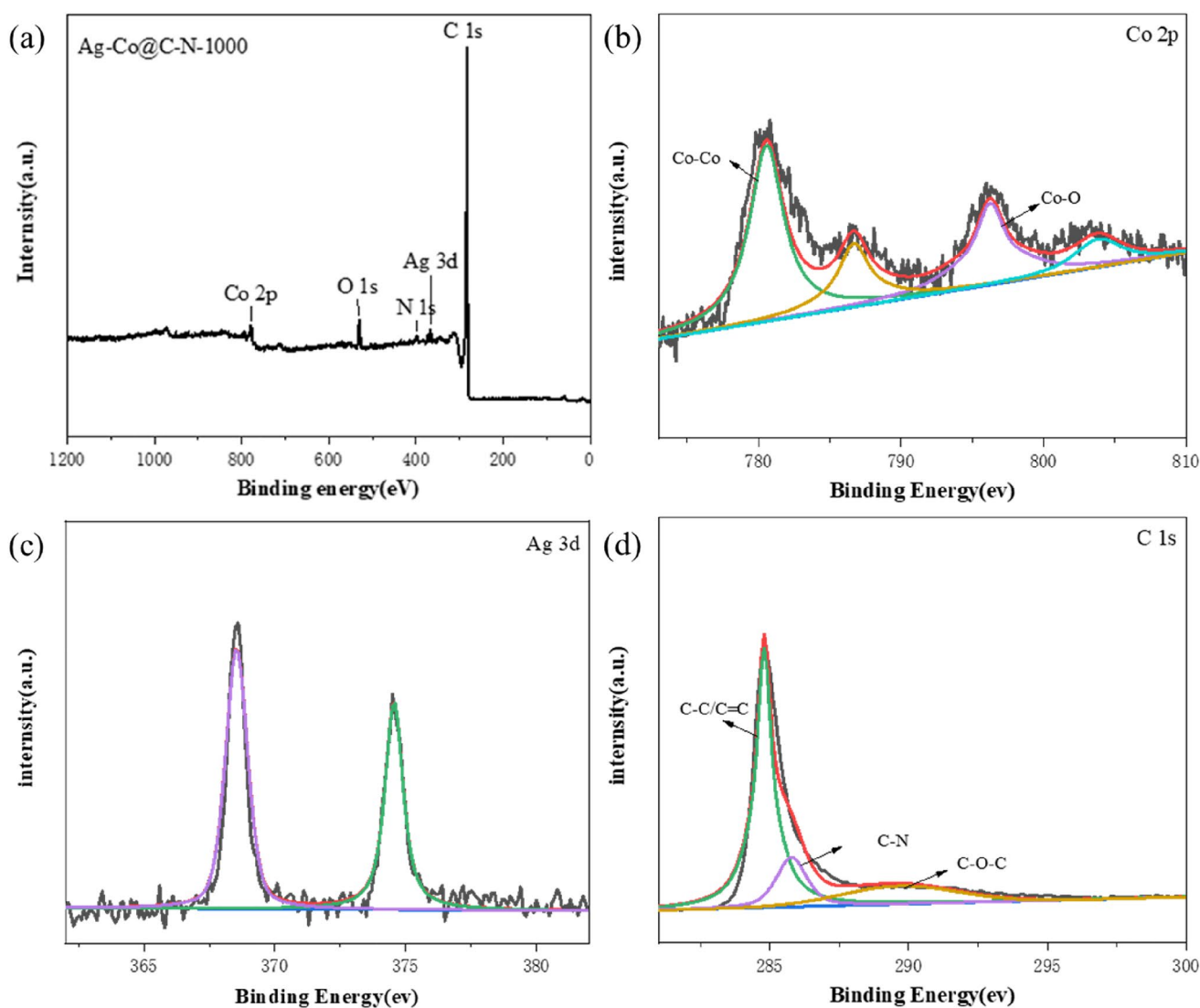


**Fig. 4** a Full survey XPS of Ag–Co@C–N–1000; high resolution XPS spectra of **b** Co 2p, **c** Ag 3d, and **d** C 1s

**Table 2** Catalytic activities of the evaluated catalysts

Entry	Catalyst	Conversion (%)	Selectivity (%)	Yield (%)
1	Co@C–N–1000	79.2	52.5	41.6
2	Ag–Co@C–N–600	94.7	77.0	72.9
3	Ag–Co@C–N–800	100	77.7	77.7
4	Ag–Co@C–N–1000	100	89.8	89.8

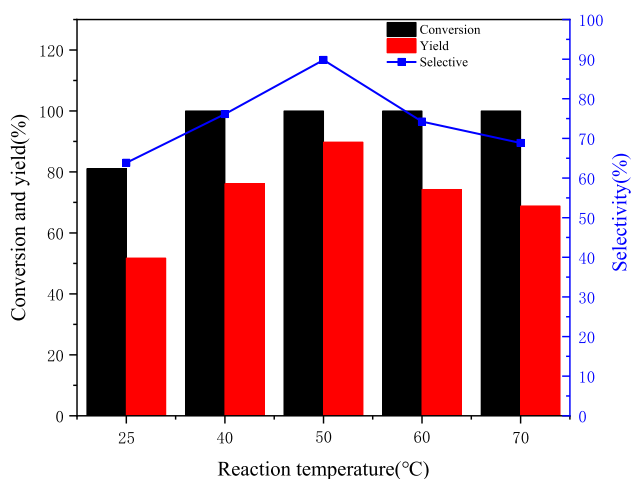
Reaction conditions: 2.5 mmol 4-chloronitrobenzene, 0.5 g hydrazine hydrate, 7.88 mg catalyst, 2.5 mL ethanol (solvent),  $t = 30$  min,  $T = 50$  °C

50 °C. At 60 and 70 °C, the product yields were 74.3% and 68.9%, respectively. The observed trends might be explained by insufficient activation-energy requirements of the system at low temperatures, resulting in a slow reaction rate and low conversion rate, and excessive hydrogenation of 1,2-Bis(4-chlorophenyl)diazene oxides at high temperatures, with generation of by-products such as azobenzene or aniline that reduce the product yield. Therefore, the optimum reaction temperature was 50 °C.

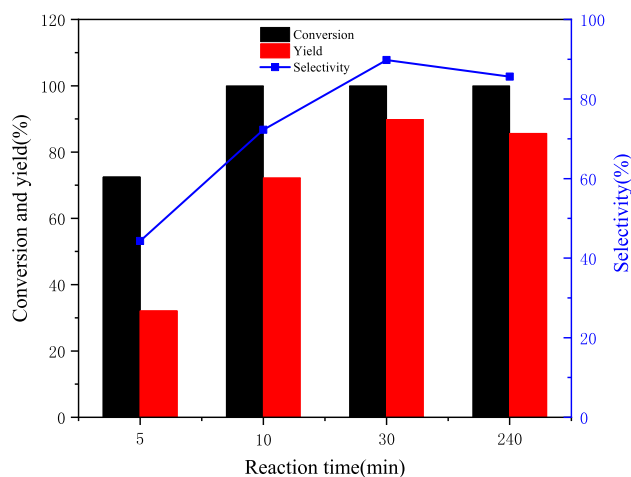
Next we researched the effect of time on the catalytic reaction system. The catalytic performances at different reaction times are compared in Fig. 6. The initial stage

**Table 3** Influences of different factors on the catalytic performance of Ag–Co@C–N-1000

Entry	Solvent	Temperature (°C)	Catalyst dosage (wt%)	Time (min)	Conversion (%)	Selectivity (%)	Yield (%)
1	Ethanol	50	0	30	0	0	0
2	Ethanol	25	2	5	46.7	40.4	18.9
3	Ethanol	25	2	10	70.7	52.4	37.0
4	Ethanol	25	2	30	81.0	63.9	51.8
5	Ethanol	25	2	240	100	83.3	83.3
6	Ethanol	40	2	30	100	76.1	76.1
7	Ethanol	50	2	5	72.5	44.3	32.1
8	Ethanol	50	2	10	100	72.3	72.3
9	Ethanol	50	2	30	100	89.8	89.8
10	Ethanol	50	2	240	100	85.6	85.6
11	Ethanol	60	2	30	100	74.3	74.3
12	Ethanol	70	2	5	93.2	71.3	66.5
13	Ethanol	70	2	10	100	78.9	78.9
14	Ethanol	70	2	30	100	68.9	68.9
15	Dichloromethane	50	2	30	52.1	3.3	1.7
16	Ethyl acetate	50	2	30	44.9	1.8	0.8
17	Tetrahydrofuran	50	2	30	43.7	4.2	1.8

**Fig. 5** Effect of reaction temperature on the catalytic performance of Ag–Co@C–N-1000

of the reaction typically includes an induction period of approximately 10 min. During the induction period, the reaction rate was extremely low because hydrazine hydrate

**Fig. 6** Effect of reaction time on the catalytic performance

must be adsorbed and activated on Ag–Co@C–N-1000. The reaction rate then increased. The conversion rate of 4-nitrochlorobenzene conversion reached 100.0% after 10 min and remained unchanged thereafter. Meanwhile,



the product yield initially increased from 72.3% at 5 min to 89.8% at 30 min. As the reaction proceeded to 240 min, the yield decreased slightly to 85.6%, possibly because it was compromised by over-hydrogenation of 1,2-Bis(4-chlorophenyl)diazene oxide to 4,4'-dichloroazobenzene and p-chloroaniline.

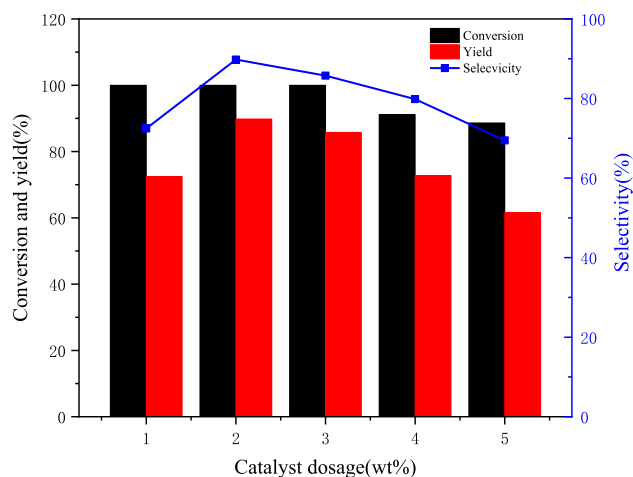
As for the effects of ethanol, dichloromethane, ethyl acetate, and tetrahydrofuran solvents on the catalytic reaction with Ag–Co@C–N-1000. The 1,2-Bis(4-chlorophenyl)diazene oxide yields were very low in all solvents except ethanol, and the raw-material conversion rates were only around 40–50%. Almost all of the reactions led to p-chloroaniline. Therefore, the type of solvent exerts an important influence on the catalytic reaction activity. The ethyl acetate, dichloromethane and tetrahydrofuran solvents accelerated the conversion of 1,2-Bis(4-chlorophenyl)diazene oxide to p-chloroaniline, thus reducing the yield of the desired product. The best solvent for this reaction was ethanol.

Figure 7 shows the effect of catalyst dosage on the catalytic performance of Ag–Co@C–N-1000. In the absence of catalyst, the reaction cannot proceed. As the catalyst dosage increased from 1 to 2 wt%, the raw-material conversion rate maintained at 100% but the product yield increased from 72.5 to 89.8%, indicating that Ag–Co@C–N-1000 played a key role in the reductive coupling of 4-nitrochlorobenzene to 1,2-Bis(4-chlorophenyl)diazene oxide. Increasing the number of active sites accelerated the reaction speed and enhanced the adsorption and conversion of the intermediate. When the catalyst dosage exceeded 2 wt%, the yield started to decline, reaching 61.6% at 5 wt%. The conversion rate

of feedstock also decreased, from 100% at 2 wt% to 88.6% at 5 wt%. The decline in conversion rate began at 4 wt%, possibly because a large amount of 4-nitrochlorobenzene was stored in the holes of excessive catalyst, reducing the utilization rate of the raw materials. Meanwhile, the yield declined because excessive catalyst promoted the excessive hydrogenation of azoxybenzenes, leading to the conversion of raw materials into by-products such as aniline. Hence, the optimum catalyst dosage was 2 wt%.

After exploring the optimal reaction conditions, we studied the catalytic activity of Ag–Co@C–N-1000 for different nitro compounds. The catalytic performances for nitroaromatic hydrocarbons with different substituents are compared in Table 4. The catalyst maintained good catalytic performance with high yields and conversion rates for nitrobenzene with an electron-donating group and an electron-absorbing halogen. Especially for para-halogen substitution, 100% of the raw material was converted after 30 min of reaction and the yield exceeded 89%. The catalyst also showed good catalytic activity for nitrobenzene with o- and m-methyl substituents, but the selectivity of the raw material was slightly reduced and a small amount of aniline was formed in the reaction with this type of substitution.

Finally, we tested the reusability of the Ag–Co@C–N-1000 catalyst under the optimized conditions (see Fig. 8). After five cycles, the 4-nitrochlorobenzene conversion decreased from 100 to 86.6% and the 1,2-Bis(4-chlorophenyl)diazene oxide yield was 74.6%, slightly lower than the initial yield (89.8%). This result indicates the high reusability performance of the catalyst. The slight decrease in activity was mainly attributed to weight loss during the catalyst recovery process.



**Fig. 7** Effect of catalyst dosage on the catalytic performance of Ag–Co@C–N-1000

## 4 Conclusion

This study investigated a series of Ag-based catalysts supported on ZIF-67-derived Ag–Co@C–N. The catalysts performed as effective bifunctional catalysts for the reductive coupling of nitroaromatics to azoxybenzenes with hydrazine hydrate. Ag–Co@C–N-1000 achieved the optimum catalytic performance, with a nitroaromatic conversion of 100% and an azoxybenzene selectivity of up to 89.8% after 30 min at 50 °C in a reductant of 0.5 g hydrazine hydrate. The catalytic activity of Ag–Co@C–N-1000 was not significantly reduced after five cycles. This work offers a promising method for the green reduction of nitroaromatics to azoxybenzenes under mild conditions.

**Table 4** Catalytic performances of Ag-Co@C-N-1000 on various nitrobenzene derivatives

Entry	Substrate	Product	Conversion (%)	Selectivity (%)	Yield (%)
1			100	89.8	89.8
2			100	93.2	93.2
3			100	69.8	68.8
4			100	83.9	83.9
5			91.2	79.9	72.9
6			90.6	79.9	72.4
7			86.3	86.7	74.8

Reaction conditions: 2.5 mmol substrate, 7.88 mg catalyst, 2.5 mL ethanol (solvent), 30 min, 50 °C

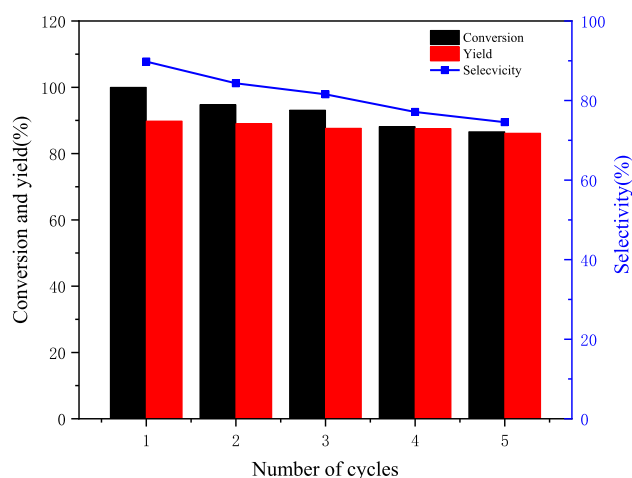


**Fig. 8** Reusability performance of the Ag–Co@C–N-1000 catalyst

**Supplementary Information** The online version contains supplementary material available at <https://doi.org/10.1007/s10562-023-04311-4>.

**Acknowledgements** This work was financially supported by the Scientific Research Project of Education Department of Hubei Province (D20181507), the Science Foundation of Wuhan Institute of Technology (K201509, K201805) and the Graduate Innovative Fund of Wuhan Institute of Technology (CX2021153).

## References

- Wibowo M, Ding L (2020) Chemistry and biology of natural azoxy compounds. *J Nat Prod* 83:3482–3491
- Combata D, Concepción P, Corma A (2014) Gold catalysts for the synthesis of aromatic azocompounds from nitroaromatics in one step. *J Catal* 311:339–349
- Zhao J-X, Chen C-Q, Xing C-H et al (2020) Selectivity regulation in Au-catalyzed nitroaromatic hydrogenation by anchoring single-site metal oxide promoters. *ACS Catal* 10:2837–2844
- Tao Y, Singh B, Jindal V, Tang Z, Pescarmona PP. Niobium oxide prepared through a novel supercritical-CO<sub>2</sub>-assisted method as a highly active heterogeneous catalyst for the synthesis of azoxybenzene from aniline. *Green Chemistry*. 2019;21: 5852–5864.
- Thota A, Wang Q, Liu P, Jian Z. Highly electrochemical active composites based on capacitive graphene/aniline oligomer hybrid for high-performance sustainable energy storage devices. *Electrochimica Acta*. 2021;368.
- Han S, Cheng Y, Liu S et al (2021) Selective oxidation of anilines to azobenzenes and azoxybenzenes by a molecular Mo oxide catalyst. *Angew Chem Int Ed* 60:6382–6385
- Chen YF, Chen J, Lin LJ, Chuang GJ (2017) Synthesis of azoxybenzenes by reductive dimerization of nitrosobenzene. *J Org Chem* 82:11626–11630
- Pahalagedara MN, Pahalagedara LR, He J et al (2016) Room temperature selective reduction of nitrobenzene to azoxybenzene over magnetically separable urchin-like Ni/Graphene nanocomposites. *J Catal* 336:41–48
- Merino E (2011) Synthesis of azobenzenes: the coloured pieces of molecular materials. *Chem Soc Rev* 40:3835
- Belgacem AGMN (1997) Furans in polymer chemistry. *Prog Polym Sci* 22:1203–1379
- Ghosh S, Acharyya SS, Sasaki T, Bal R (2015) Room temperature selective oxidation of aniline to azoxybenzene over a silver supported tungsten oxide nanostructured catalyst. *Green Chem* 17:1867–1876
- Zhou B, Song J, Wu T et al (2016) Simultaneous and selective transformation of glucose to arabinose and nitrosobenzene to azoxybenzene driven by visible-light. *Green Chem* 18:3852–3857
- Nishiyama Y, Fujii A, Mori H (2019) Selective synthesis of azoxybenzenes from nitrobenzenes by visible light irradiation under continuous flow conditions. *Reaction Chemistry & Engineering* 4:2055–2059
- Senthil Raja D, Huang C-L, Chen Y-A, Choi Y, Lu S-Y (2020) Composition-balanced trimetallic MOFs as ultra-efficient electrocatalysts for oxygen evolution reaction at high current densities. *Appl Catal B* 279:119375
- Noor T, Pervaiz S, Iqbal N et al (2020) Nanocomposites of NiO/CuO based MOF with rGO: an efficient and robust electrocatalyst for methanol oxidation reaction in DMFC. *Nanomaterials (Basel)* 10:1601
- Huang Z, Liu J, Xiao Z et al (2018) A MOF-derived coral-like NiSe@NC nanohybrid: an efficient electrocatalyst for the hydrogen evolution reaction at all pH values. *Nanoscale* 10:22758–22765
- Li H, Ke F, Zhu J (2018) MOF-derived ultrathin cobalt phosphide nanosheets as efficient bifunctional hydrogen evolution reaction and oxygen evolution reaction electrocatalysts. *Nanomaterials (Basel)* 8:89
- Bhatt MD, Lee JY (2020) Advancement of platinum (Pt)-free (non-Pt precious metals) and/or metal-free (non-precious-metals) electrocatalysts in energy applications: a review and perspectives. *Energy Fuels* 34:6634–6695
- Park KS, Ni Z, Côté AP, Choi JY, Huang R, Uribe-Romo FJ, Chae HK, O’Keeffe M, Yaghi OM. Exceptional chemical and thermal stability of zeolitic imidazolate frameworks. *Proceedings of the National Academy of Sciences*. 2006;103.
- Phan A, Doonan CJ, Uribe-Romo FJ, Knobler CB, O’keeffe M, Yaghi OM. Synthesis, Structure, and carbon dioxide capture properties of zeolitic imidazolate frameworks. *Accounts Of Chemical Research*. 2010;43: 58–67.
- Wu SC, Chang PH, Chou SH, Huang CY, Liu TC, Peng CH (2020) Waffle-like carbons combined with enriched mesopores and highly heteroatom-doped derived from sandwiched MOF/LDH/MOF for high-rate supercapacitor. *Nanomaterials (Basel)* 10:2388
- Liu J, Ran Z, Cao Q, Ji S (2021) Preparation of MIL-88B(Fex, Co1-x) catalysts and their application in one-step liquid-phase methanol oxidation to methyl formate using H<sub>2</sub>O<sub>2</sub>. *Chin J Catal* 42:2254–2264
- Li B, Sun K, Guo Y, Tian J, Xue Y, Sun D (2013) Adsorption kinetics of phenol from water on Fe/AC. *Fuel* 110:99–106
- Anshori I, Nuraviana Rizalputri L, Rona Althof R et al (2021) Functionalized multi-walled carbon nanotube/silver nanoparticle (f-MWCNT/AgNP) nanocomposites as non-enzymatic electrochemical biosensors for dopamine detection. *Nanocomposites* 7:97–108
- Xiong P, Zhao X, Xu Y (2018) Nitrogen-doped carbon nanotubes derived from metal-organic frameworks for potassium-ion battery anodes. *Chemsuschem* 11:202–208
- Ding J, Chen M, Du X et al (2019) Visible-light-driven photoreduction of CO<sub>2</sub> to CH<sub>4</sub> with H<sub>2</sub>O over amine-functionalized MIL-125(Ti). *Catal Lett* 149:3287–3295

27. Jing Y, Lei Q, Xia C et al (2020) Synthesis of Ag and AgCl co-doped ZIF-8 hybrid photocatalysts with enhanced photocatalytic activity through a synergistic effect. *RSC Adv* 10:698–704
28. Bai C, Li A, Yao X, Liu H, Li Y (2016) Efficient and selective aerobic oxidation of alcohols catalysed by MOF-derived Co catalysts. *Green Chem* 18:1061–1069
29. Paul B, Vadivel S, Yadav N, Dhar SS (2019) Room temperature catalytic reduction of nitrobenzene to azoxybenzene over one pot synthesised reduced graphene oxide decorated with Ag/ZnO nanocomposite. *Catal Commun* 124:71–75
30. Qian H, Zhu M, Wu Z, Jin R (2012) Quantum sized gold nano-clusters with atomic precision. *Acc Chem Res* 45:1470–1479
31. Wei X, Li N, Zhang X (2018) Co/CoO/C@B three-phase composite derived from ZIF67 modified with NaBH<sub>4</sub> solution as the electrocatalyst for efficient oxygen evolution. *Electrochim Acta* 264:36–45
32. Tan BJ, Klabunde KJ, Sherwood PM (1990) X-ray photoelectron spectroscopy studies of solvated metal atom dispersed catalysts. Monometallic Iron and Bimetallic Iron-Cobalt Particles on Alumina *Chemistry of Materials* 2:186–191
33. Chuang TJ, Brundle CR, Rice DW (1976) Interpretation of the X-ray photoemission spectra of cobalt oxides and cobalt oxide surfaces. *Surf Sci* 59:413–429
34. Ledeuil JB, Uhart A, Soule S, Allouche J, Dupin JC, Martinez H (2014) New insights into micro/nanoscale combined probes (nanoAuger, muXPS) to characterize Ag/Au@SiO<sub>2</sub> core-shell assemblies. *Nanoscale* 6:11130–11140

**Publisher's Note** Springer Nature remains neutral with regard to jurisdictional claims in published maps and institutional affiliations.

Springer Nature or its licensor (e.g. a society or other partner) holds exclusive rights to this article under a publishing agreement with the author(s) or other rightsholder(s); author self-archiving of the accepted manuscript version of this article is solely governed by the terms of such publishing agreement and applicable law.